Supplementary material

S1. Effective depth resolution of the CFA records

Effective depth resolution of the CFA records was evaluated based on the time it took for the various measurement lines in the system to respond to an abrupt change in concentration level. Following the approach in Bigler et al. (2011), response times were calculated as the average time required for the system to transition from a blank water standard to the highest calibration standard plateau, using the 10% and 90% levels of the transition curve. From the employed melt rate of 3 cm/min, response times were then converted to equivalent response depths as a measure for the effective depth resolution. For the RICE CFA set-up, the conductivity record has the highest effective resolution of 0.8 cm, closely followed by black carbon (Table S1).

	Response time (s)	Response depth (cm)	Missing data fraction
Conductivity	15 ± 2	0.8 ± 0.1	6%
Acidity	38 ± 3	1.9 ± 0.2	17%
Calcium	49 ± 6	2.5 ± 0.3	9%
Black carbon	20 ± 3	1.0 ± 0.2	<1%
Insoluble dust particles	17 ± 3	1.0 ± 0.2	8%

Table S1: Response times for the CFA system to transition between the blank water level and a calibration standard plateau, and the equivalent response depths. Core breaks, contamination, measurement errors etc. gave rise to sections of missing data, these comprising from 1% to 17% of the total length of the record. Below 129 m, the dust record was extensively contaminated by drill liquid, and the missing data fraction is calculated for the uncontaminated top part only.

S2. StratiCounter settings and procedure

StratiCounter was initialized based on a preliminary set of manual layer annotations (Fig. 6a) within a selected depth interval (40-150 m). The manual annotations were used to produce a set of generalized templates for an annual layer in the various impurity records. We note that the manually-counted timescale was observed to have a bias towards counting too few layers, resulting in an age for the Pleiades tephra that is a few decades younger than observed in WAIS Divide. Applying the Expectation-Maximization algorithm (e.g. Gupta and Chen 2010), StratiCounter continuously updates and refines the statistical description of an annual layer, thereby allowing for changes in layer characteristics with depth (Winstrup, 2016; Winstrup et al., 2012). To further increase the independence of the StratiCounter timescale from the preliminary manual interpretation, in a final step the entire timescale was reevaluated using an improved set of layer templates derived from the algorithm output.

Rapid thinning of layers with depth in the core necessitated slight changes in StratiCounter settings with depth. We therefore divided the record into four sections: an upper (42-180 m), an upper middle (165-250 m), a lower middle (240-300 m), and a lower section (280-344 m). Overlap sections served as base for comparison between the runs, which were found to contain only minor differences. Within these sections, the results from the deeper section were used to produce the final timescale.

For the uppermost section (42-180 m), performance of the algorithm was tested using a variety of algorithm settings, which all resulted in very similar timescales (±10 years at 165 m). The final version was chosen as the timescale in best agreement with the WD2014 age of the Pleiades tephra horizon (Dunbar et al., 2010) found at 165 m of depth (Wheatley and Kurbatov, 2017). Proceeding to the deeper sections, the algorithm settings were kept as similar as possible to those employed for the upper part.

The main change in settings with depth was the averaging distance employed to produce a lower-resolution record from the original 1-mm resolution CFA records, performed before automatic layer identification. Section delimitations were selected based on estimated layer thicknesses obtained from methane matching to the WAIS Divide ice core (Lee et al., 2018), and chosen so that an average layer consisted of approximately 10-15 individual data points. Accordingly, the averaging distance was successively reduced from 1.5 cm to 0.5 cm to account for the general decrease in layer thicknesses with depth (Table S2). Note that the averaging distance applied for the deepest section is less than the effective resolution of even the highest-resolution impurity records (Table S1), meaning that successive averaged data points are significantly correlated.

StratiCounter was run based on the full suite of CFA records: Black carbon, acidity, calcium, conductivity, and dust (topmost section only). The dust record was excluded for the lower sections due to drill liquid contamination. The impurity records were weighted so that records of large similarity (e.g. calcium and conductivity) were not treated as independent data series, and with added emphasis on the black carbon, which displayed the most pronounced annual signal (Table S2). Before analysis, extreme peaks caused by measurement noise and processing errors were removed from the data series. These were further standardized using z-scores based on the logarithm of the impurity concentrations in order to reduce interannual variability in layer signal.

Section	**42.34–180 m** (42.34-165 m)	**165-250 m** (165-240 m)	**240-300 m** (240-280 m)	**280-350 m** (280-343.7 m)
Depth resolution (cm)	1.5	1.0	0.75	0.5
Weights of impurity series				
Black carbon	1	1	1	1
Acidity	0.5	0.5	0.5	0.5
Dust	0.5	0	0	0
Calcium	0.25	0.25	0.25	0.25
Conductivity	0.25	0.25	0.25	0.25

Table S2: StratiCounter settings for each depth range (in parenthesis is given the interval for which the results were used to produce the final combined timescale): Interpolated depth resolution of the impurity records before automated layer identification, and weighting of the various impurity records in the StratiCounter algorithm.

S3. The RICE density profile

Measured densities for the RICE core (Fig. S1) show good agreement with a modelled density profile calculated from a steady-state Herron-Langway densification model (Herron and Langway, 1980) when using appropriate values for the initial snow density (410 kg m^{-3}; within the range measured in adjacent snow pits), surface temperature (-23.5°C; consistent with borehole temperatures (Bertler et al., 2018)), and accumulation rate (0.22 m w.e yr^{-1}). The measured density profile was extended to the surface using the modelled densities. We note that the initial densification in the Herron-Langway model is parameterized as a linear function of depth, depending only on initial snow density and surface temperature.

At intermediate depths (50-120 m), the observed density profile has slightly denser snow than predicted by the Herron-Langway model, and, as a result, the firn-ice transition is reached at significantly shallower depths than predicted by the model. This difference may indicate that a steady-state assumption is invalid, or it may be due to the additional vertical strain present at divide locations (Kingslake et al., 2014).

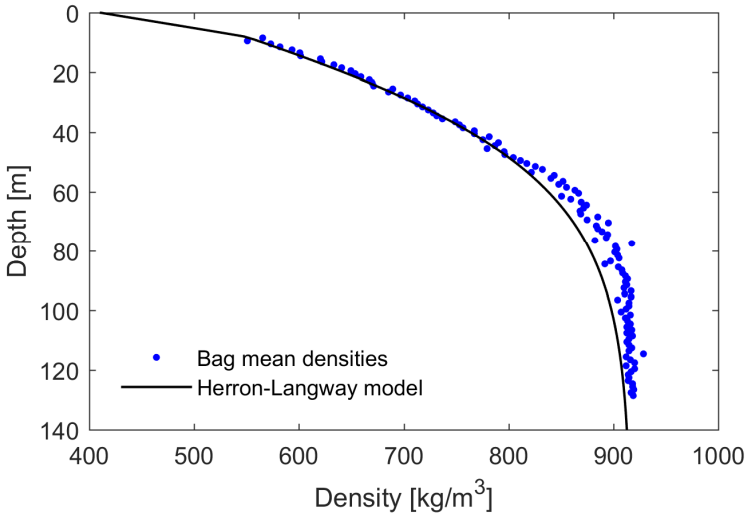

Figure S1: Measured and modelled density profile for the RICE core.

S4: Modeling of the thinning function for reconstructing the accumulation rate history

Model setup

To calculate the thinning function, we employ a one-dimensional ice-flow model run at an annual time step, which tracks the cumulative thinning of an ice layer. At each time step, the full-depth vertical velocity profile is found by scaling the shape of the vertical profile (discussed below) to the surface velocity. The vertical surface velocity is determined as the sum of the accumulation rate and the rate of ice-sheet thinning, the latter assumed constant in time. Forced with a time-dependent accumulation rate, the model computes the thinning function based on integration of the vertical strain over time. Starting from an assumption of constant accumulation, we iterate until the accumulation history and thinning function are consistent. While the surface vertical velocity likely does not vary at annual timescales, the resulting thinning functions are smooth, and no improvement comes from using a smoothed accumulation history.

Typical shapes of respectively "pure divide flow" and "flank flow" vertical velocity profiles at Roosevelt Island (Figure S2) were found by fitting Lliboutry-type ice-flow shape parametrizations (Lliboutry, 1979) to englacial velocities measured from repeat phase-sensitive radar measurements (Kingslake et al., 2014). However, no velocity measurements were possible in the upper 90m due to effects of firn compaction, meaning that some assumptions on the near-surface velocities were required. We therefore computed the thinning function using two different parametrizations of the velocity profile.

As discussed in the main text, the divide may have migrated in the past, and the vertical velocity profiles experienced by the ice in the core may thus have changed through time. To account for this, we follow Nereson and Waddington (2002) and describe the vertical velocity profiles as time-varying linear combinations of the divide and flank profiles. This allows a smooth variation in the vertical velocity profiles through time.

Uncertainties

For RICE, there are three primary sources of uncertainty in estimating the thinning function: 1) the shape of the vertical velocity profile where no measurements exist in the upper 90m, 2) the history of changes in the vertical velocity profile as the divide may have migrated, and 3) the rate of ice-sheet thickness change. Each source of uncertainty is discussed below.

The total uncertainty is estimated by calculating the thinning function using two possible parametrizations of the vertical velocity profiles, two divide-history scenarios, and three plausible rates

of ice-sheet thinning, described below. The resulting accumulation histories are shown in Figure S3. We define the uncertainty as the full range of these 12 scenarios, which we interpret as a 95% confidence interval.

The vertical velocity profile

Following the work of Lliboutry (1979), the vertical ice-flow velocity profiles (w) at normalized depth (ζ) can be parameterized using the vertical velocity at the surface (w_s) and a shape factor (p):

$$w(\zeta) = w_s \left(1 - \frac{p+2}{p+1}\zeta + \frac{1}{p+1}\zeta^{p+2}\right)$$

Fitting to the vertical velocities measured for divide-like flow at Roosevelt Island (Fig. S2, red asterisks), Kingslake et al. (2014) found the best fit with a surface velocity (w_s) of 0.27 m/yr and p = -0.78 (Fig. S2, red dashed line). However, this fit has two limitations: i) it over-predicts the vertical velocity at mid-depths, and ii) given a recent accumulation rate of 0.24 m ice eq./yr, it implies a thinning of the ice sheet of 0.03m/yr. This amount of ice-sheet thickness change is at the upper limit of what is plausible given the observed structure of the Raymond Arch.

A more negative p value, p = -1.22, better matches the vertical velocity measurements, but requires a larger surface velocity, which can be excluded. As noted by Kingslake et al. (2014), the vertical velocity profile is near-linear in the upper part of the measurements. We therefore construct a second parametrization of the velocity profile as follows: We employ the Lliboutry fit using p = -1.22, but replace the top part with a linear velocity increase towards the surface, starting at 155m ice equivalent depth (Fig. S2, solid red line). This is our preferred vertical velocity profile for divide-type flow at Roosevelt Island. The associated downwards surface velocity of 0.26m/yr corresponds to an ice-sheet thinning rate of 0.02 m/yr, which is consistent with the characteristics of the Raymond Arch.

For flank-type flow, the misfit to the measured vertical velocity measurements was minimized using w_s = 0.24 m/yr and p = 4.16 (Fig. S2, blue line), for which good agreement between measurements and model was obtained (Kingslake et al., 2014).

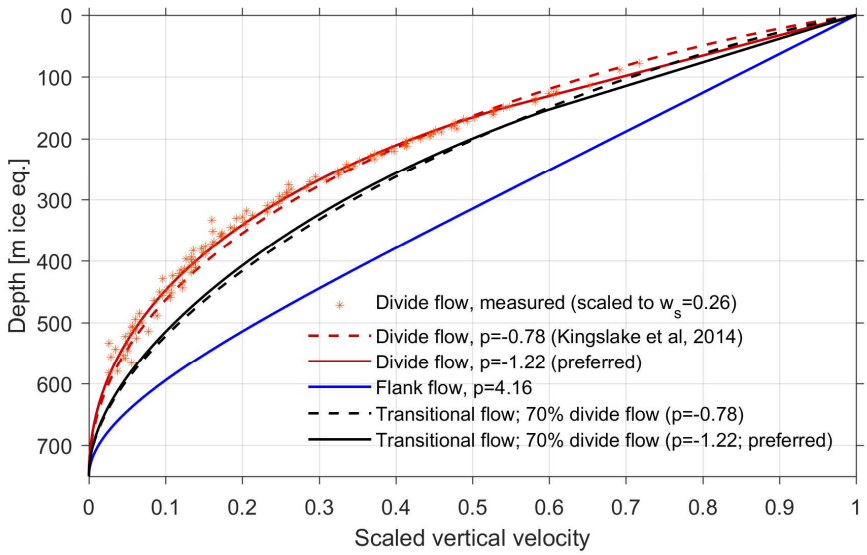

Figure S2: Vertical velocity profiles (scaled to the surface velocity, w_s) used for calculating the RICE thinning functions. Two shape parametrizations for divide flow were used (red lines), both derived from fitting to the measured vertical velocities (Kingslake et al., 2014). Our preferred fit (solid red line) improves the overall misfit and does not have a bias at mid-depth. For the flank-flow profile (blue), we used the fit from Kingslake et al. (2014). Also shown are vertical velocity profiles for transitional flow (black lines), calculated as a linear combination of the two profiles consisting of 70% divide flow and 30% flank flow, as appropriate for the majority of the RICE core.

Divide migration history

As discussed in the main text, there is ambiguity in the history of divide migration, and how it has influenced the vertical strain history at the core site. The main cause of uncertainty is the inference of maximum near-surface strain rates, i.e. the most "divide-like" flow, being slightly offset to the east of the present topographic divide (Kingslake et al., 2014; Fig 6b), where the ice core was drilled. It may therefore be that the drill site is not located at the present location of full divide-like flow. However, we note that there is considerable uncertainty in the pRES measurements of vertical strain rates, and that these do not extent to within 90m of the surface. In the near-surface layers, the peak of the Raymond Arch tilts towards to the modern summit, suggesting that the divide (and the location of maximum divide-flow) has migrated towards the current topographic summit in the most recent past. We consider this to be the most likely ice-divide migration and corresponding flow history.

In our preferred scenario with recent divide migration, the older ice in the core experienced a transitional flow regime somewhere between flank and ice-divide flow, but is now experiencing full divide flow. Starting from ~120m (~1500 CE), the amplitude of the Raymond Arch at the core site is approximately 70% of the peak amplitude. Prior to 1512 CE (500 years before the core was drilled), we therefore used a vertical velocity profile appropriate for divide-flank (70%/30%) transitional-type ice flow (Fig. S2; black lines). Over the following 250 years (1512-1762 CE), the ice divide was assumed to migrate to its present position, while the vertical velocity profile transitioned to full divide-type flow.

To account for the uncertainty in divide migration during the most recent past, the thinning function was also calculated for the following second scenario: We assume that maximum divide-flow has always been offset from the topographic summit, and thus that the ice in the core has experienced entirely transitional flow.

Ice-sheet thinning rate

A third source of uncertainty is the amount of ice-sheet thickness change. Changes in ice-sheet thickness will affect the vertical velocity, causing more vertical strain of layers in a thinning ice sheet. For the deeper part of the ice core, changing the prescribed thinning rate is the most important source of uncertainty for the accumulation rate reconstruction (Figure S3, blue lines).

We assessed the plausible range of ice-sheet thickness change both by fitting the measured vertical velocity profiles and by modeling the amplitude of the Raymond Arch. While 2D modeling of the dated internal stratigraphy of Roosevelt Island is on-going, we find that the likely range of ice-sheet thickness change is 1 to 3 cm/year, with 2 cm/year being the preferred amount.

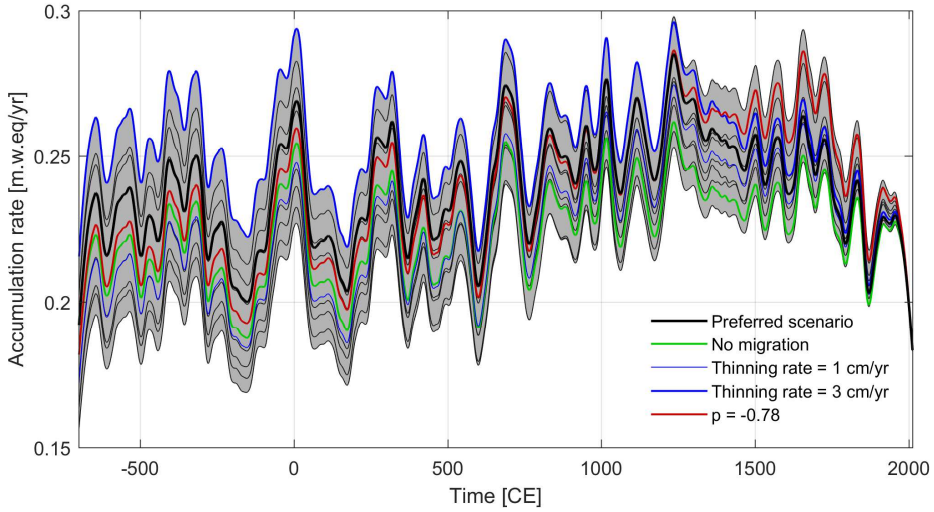

Figure S3: Reconstructed accumulation histories according to the 12 scenarios described in the text. The 95% confidence interval (grey area) is taken as the envelope of all accumulation histories. Colored lines show the impact on the accumulation history from the various sources of uncertainty, when changing one of these at a time relative to the preferred scenario (thick black line).

S5: Volcanic matching to WAIS Divide

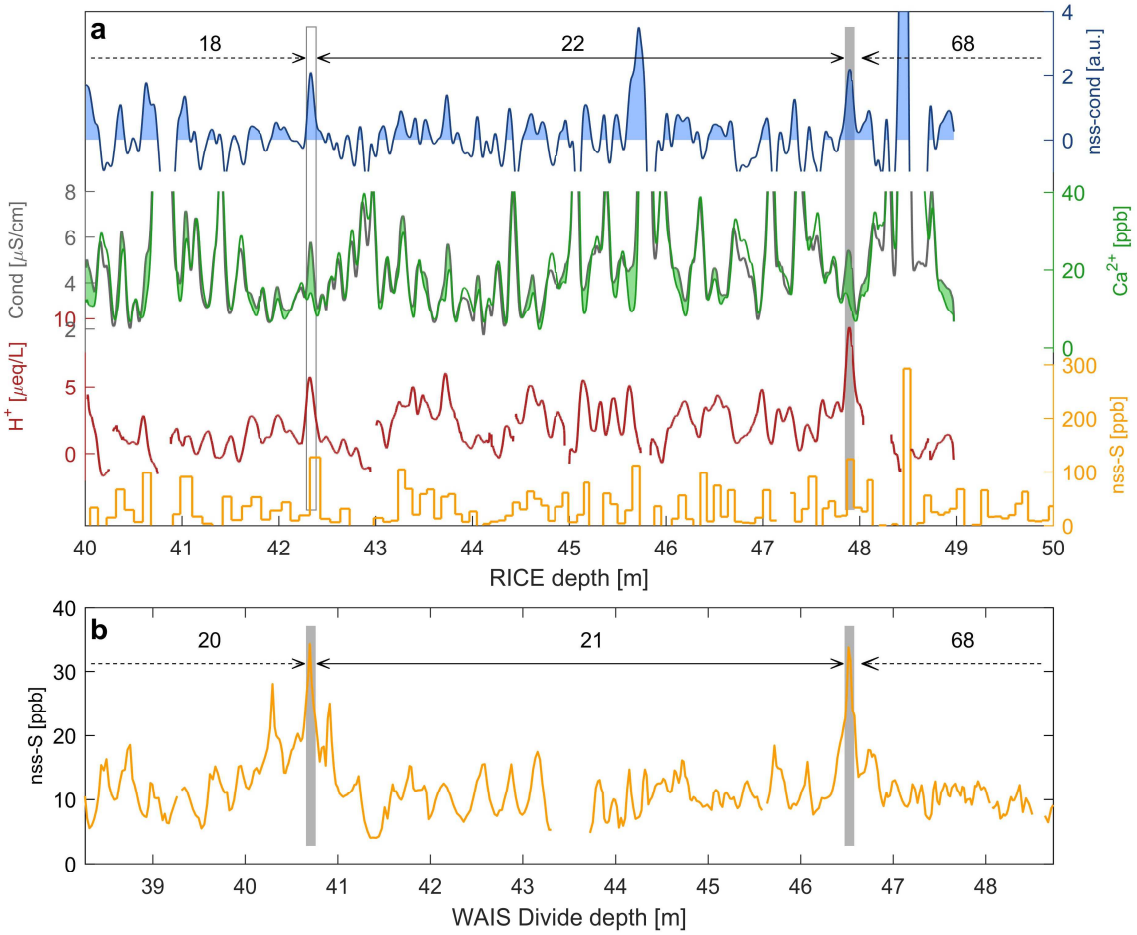

Figure S4: Volcanic matching between **a)** RICE and **b)** WAIS Divide for a recent section, including the Krakatau (1883 CE) and Makian (1861 CE) volcanic horizons. Vertical bars indicate volcanic match points (Table 2), and numbers denote the number of annual layers between match points in the two records according to their respective timescales. Mean peak height for Krakatau (white bar) does not exceed 2σ of the internal variability (mean of all available records), but is clearly visible when e.g. comparing the Ca^{2+} and conductivity records directly. Green area shows the conductivity-to-calcium excess directly from the two records, with the resulting non-sea-salt conductivity record shown in the top panel.

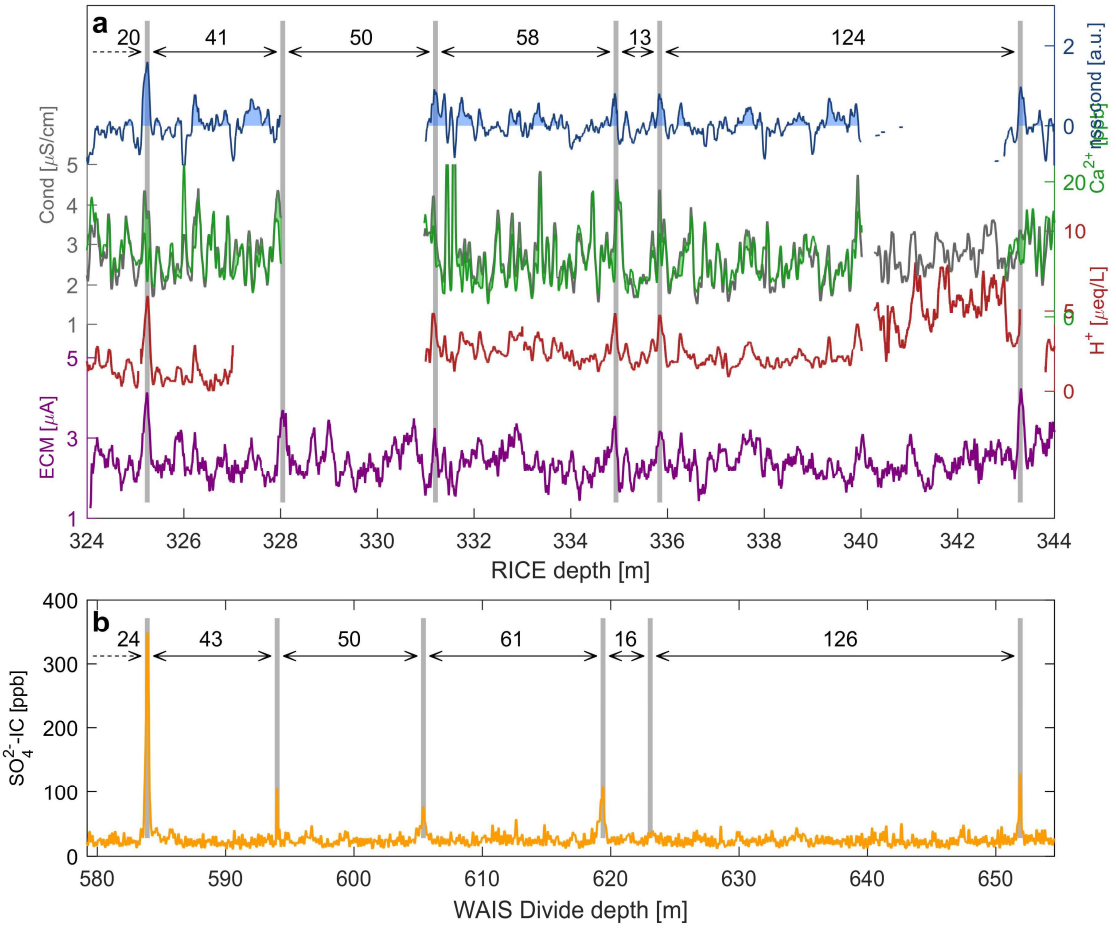

Figure S5: Volcanic matching between **a)** RICE and **b)** WAIS Divide for the deepest part of the RICE record considered here. Vertical bars indicate volcanic match points (Table 2), and numbers denote the number of annual layers between match points in the two records according to their respective timescales. For this section, the RICE17 timescale shows a small, but distinct, bias towards counting fewer layers than present in WD2014.

Supplementary references

Bertler, N. A. N., Conway, H., Dahl-Jensen, D., Emanuelsson, D. B., Winstrup, M., Vallelonga, P. T., Lee, J. E., Brook, E. J., Severinghaus, J. P., Fudge, T. J., Keller, E., Baisden, W. T., Hindmarsh, R. C. A., Neff, P. D., Blunier, T., Edwards, R., Mayewski, P. A., Kipfstuhl, S., Buizert, C., Canessa, S., Dadic, R., Kjær, H. A., Kurbatov, A. V., Zhang, D., Waddington, E. D., Baccolo, G., Beers, T., Brightley, H. J., Carter, L., Clemens-Sewall, D., Ciobanu, V. G., Delmonte, B., Eling, L., Ellis, A. A., Ganesh, S., Colledge, N., Haines, S. A., Handley, M., Hawley, R. L., Hogan, C. M., Johnson, K. M., Korotkikh, E., Lowry, D. P., Mandeno, D., McKay, R. M., Menking, J. A., Naish, T. R., Noerling, C., Ollive, A., Orsi, A., Proemse, B. C., Pyne, A. R., Pyne, R. L., Renwick, J., Scherer, R. P., Semper, S., Simonsen, M., Sneed, S. B., Steig, E. J., Tuohy, A., Ulayottil Venugopal, A., Valero-Delgado, F., Venkatesh, J., Wang, F., Wang, S., Winski, D. A., Winton, V. H. L., Whiteford, A., Xiao, C., Yang, J. and Zhang, X.: The Ross Dipole - temperature, snow accumulation, and sea ice variability in the Ross Sea Region, Antarctica, over the past 2700 years, Clim. Past, 14, 193–214, doi:10.5194/cp-14-193-2018, 2018.

Bigler, M., Svensson, A., Kettner, E., Vallelonga, P., Nielsen, M. E. and Steffensen, J. P.: Optimization of high-resolution continuous flow analysis for transient climate signals in ice cores, Environ. Sci. Technol., 45(10), 4483–4489, doi:10.1021/es200118j, 2011.

Dunbar, N. W., Kurbatov, A. V., Koffman, B. G. and Kreutz, K. J.: Tephra Record of Local and Distal Volcanism in the WAIS Divide Ice Core, in WAIS Divide Science Meeting September 30th-October 1st, La Jolla, CA, USA, available at: https://geoinfo.nmt.edu/staff/dunbar/publications/abstracts/dakk2010.html (last access: 24 March 2019), 2010.

Gupta, M. R. and Chen, Y.: Theory and Use of the EM Algorithm, Found. Trends® Signal Process., 4(3), 223–296, doi:10.1561/2000000034, 2010.

Herron, M. M. and Langway, C. C.: Firn densification: An empirical model, J. Glaciol., 25(93), 373–385, doi:10.3189/S0022143000015239, 1980.

Kingslake, J., Hindmarsh, R. C. A., Adalgeirsdottir, G., Conway, H., Pritchard, H. D., Corr, H. F. J., Gillet-Chaulet, F., Martin, C., King, E. C., Mulvaney, R. and Pritchard, H. D.: Full-depth englacial vertical ice sheet velocities measured using phase-sensitive radar, J. Geophys. Res. Earth Surf., 119, 2604–1618, doi:10.1002/2014JF003275, 2014.

Kurbatov, A. V., Kalteyer, D. A., Dunbar, N. W., Yates, M. G., Iverson, N. A. and Bertler, N. A.: Major element analyses of visible tephra layers in the Roosevelt Island Climate Evolution Project ice core (Antarctica), Interdiscip. Earth Data Alliance, doi:10.1594/IEDA/100554, 2015.

Lee, J., Brook, E. J., Bertler, N. A. N., Buizert, C., Baisden, W. T., Blunier, T., Ciobanu, G., Conway, H., Dahl-Jensen, D., Fudge, T. J., Hindmarsh, R. C. A., Keller, E. D., Parrenin, F., Severinghaus, J. P., Vallelonga, P., Waddington, E. D. and Winstrup, M.: An 83,000 year old ice core from Roosevelt Island, Ross Sea, Antarctica, Clim. Past Discuss., 1–44, doi:10.5194/cp-2018-68, 2018.

Lliboutry, L. A.: A critical review of analytical approximate solutions for steady state velocities and temperatures in cold ice sheets, Gletscherkd. Glazialgeol, 15(2), 135–148, 1979.

Nereson, N. A. and Waddington, E. D.: Isochrones and isotherms beneath migrating ice divides, J. Glaciol., 48(160), 95–108, doi:10.3189/172756502781831647, 2002.

Winstrup, M.: A Hidden Markov Model Approach to Infer Timescales for High-Resolution Climate Archives, in Proceedings of the 30th AAAI Conference on Artificial Intelligence and the 28th Innovative Applications of Artificial Intelligence Conference, 12-17 February 2016, AAAI Press, Palo Alto, California, Phoenix, Arizona, USA, 4053–4061, P28L94: available at: https://www.aaai.org/ocs/index.php/IAAI/IAAI16/paper/view/11993/12328 (last access: 31 March 2019), 2016.

Winstrup, M., Svensson, A. M., Rasmussen, S. O., Winther, O., Steig, E. J. and Axelrod, A. E.: An automated approach for annual layer counting in ice cores, Clim. Past, 8, 1881–1895, doi:10.5194/cp-8-1881-2012, 2012.